

Self-Supervised Fine-tuning for Image Enhancement of Super-Resolution Deep Neural Networks

Alice Lucas, Santiago Lopez-Tapia, Rafael Molina and Aggelos K. Katsaggelos.

Abstract—While Deep Neural Networks (DNNs) trained for image and video super-resolution regularly achieve new state-of-the-art performance, they also suffer from significant drawbacks. One of their limitations is their tendency to generate strong artifacts in their solution. This may occur when the low-resolution image formation model does not match that seen during training. Artifacts also regularly arise when training Generative Adversarial Networks for inverse imaging problems. In this paper, we propose an efficient, fully self-supervised approach to remove the observed artifacts. More specifically, at test time, given an image and its known image formation model, we fine-tune the parameters of the trained network and iteratively update them using a data consistency loss. We apply our method to image and video super-resolution neural networks and show that our proposed framework consistently enhances the solution originally provided by the neural network.

I. INTRODUCTION

In the past decade, the application of Deep Neural Networks (DNNs) to solving inverse imaging problems has gained considerable popularity [2]. The conventional strategy used to train DNNs for such problems requires the training of a neural network $f_{\psi}(\cdot)$ which learns the optimal parameters $\tilde{\psi}$ that map any observed image y to its restored version x by completing a forward pass: $\tilde{x} = f_{\tilde{\psi}}(y)$. The observed image y is assumed to come from a known image formation model with degradation operator A , which we formulate here as $y = Ax + \epsilon$, where ϵ denotes the noise. The parameters $\tilde{\psi}$ are learned through a lengthy training stage which requires the use of a large dataset of input-output (y, x) pairs. The training data is commonly generated by applying the degradation operator A to the clean images to obtain the corresponding degraded images used for training. With this straight-forward framework combined with the fast-growing nature of Deep Learning, new state-of-the-art results for image restoration tasks are regularly achieved.

Preliminary results of this work were presented at the 2019 IEEE International Conference on Image Processing (ICIP) [1]. This work was supported in part by the Sony 2016 Research Award Program Research Project and by the National Science Foundation under grant DGE-1450006. The work of SLT and RM was supported by the Spanish Ministry of Economy and Competitiveness through project DPI2016-77869-C2-2-R and the Visiting Scholar program at the University of Granada. SLT received financial support through the Spanish FPU program. A. Lucas and A.K. Katsaggelos are with the Dept. of Electrical Engineering and Computer Science, Northwestern University, Evanston, IL, USA. S. Lopez-Tapia and R. Molina are with the Computer Science and Artificial Intelligence Department, Universidad de Granada, Spain. **This work has been submitted to the IEEE for possible publication. Copyright may be transferred without notice, after which this version may no longer be accessible.**

However, what the Deep Learning community frequently fails to expose in their publications are the failure cases of using DNNs for inverse imaging problems which may result in unnatural-looking images with unpleasant artifacts. Indeed, under certain conditions, these networks may produce images of unsatisfactory quality that are not up to the established standards. To illustrate, we detail here two common case scenarios that may arise in super-resolution.

1) *Disagreement between training and testing image formation models in super-resolution*: It is well known that a DNN trained for a specific image recovery problem will not generalize well to a test data point whose image formation model differs from the model established when synthesizing the training dataset. In the case of super-resolution (SR), for example, providing a test image downsampled by a factor of 3 to a neural network trained for performing SR of scale factor 4 will most probably introduce mild artifacts. Another example of an inconsistent image formation model in SR includes the case in which blurring of the high-resolution image prior to its downsampling was not accounted for when generating the training dataset, yet such a blurred and downsampled image is provided at the input to the network at test time [3]. Again in this case, the network is to some extent successful at increasing the resolution of its input. However, as the neural network was not trained to remove blur in its low-resolution inputs, the resulting solution suffers too from excessive blurring. Moreover, as shown in [3], training the network to also remove the blur does not guarantee optimal results, as any mismatch between the blur kernels used in training and the ones encountered during testing results in the appearance of artifacts in the SR images.

2) *Artifacts resulting from the training of Generative Adversarial Networks*: The application of the Generative Adversarial Network (GAN) [4] formulation to inverse imaging problems has resulted in solutions of previously unseen restoration quality, including SR tasks ([5], [6], [7], [8]). Despite greatly increasing the resolution of their input, GANs are also known to frequently generate unpleasant artifacts in their output. These artifacts may appear in many different shapes and forms, as they are the result of a complex relationship between "ill-behaving" cost functions and challenging training dynamics. Examples of artifacts that may be produced by GANs for VSR are shown and discussed in [5].

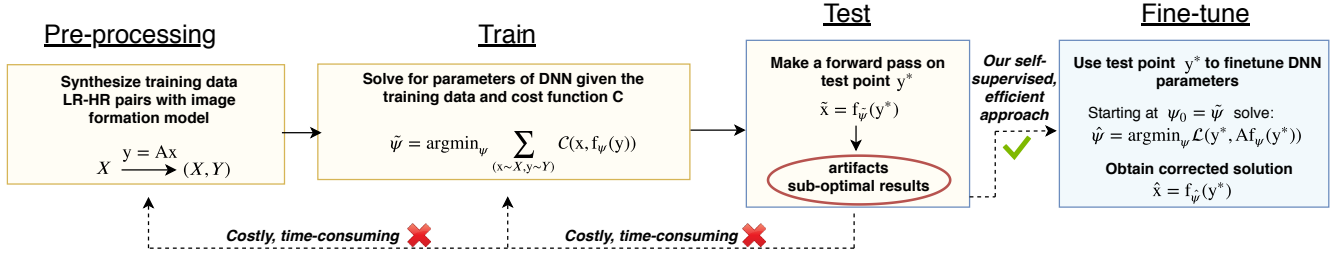


Figure 1: An illustration of our approach. We address the case when the image predicted by the DNN has artifacts. We fine-tune the parameters of the DNN using the observed data point only and avoid the cost of re-training the DNN.

As inverse imaging problems present many challenges and traditional DNNs lack robustness and generalization to the image formation model, a multitude of other scenarios that lead to substandard results could be conceived in addition to the ones described above. In the Deep Learning literature, the standard procedure to improving results consists of adapting the training set-up in an attempt to minimize, or completely remove, these artifacts accordingly. For example the prevalent approach taken to remove artifacts that arise from an unseen image formation model at test time is to re-synthesize the training dataset with the appropriate degradation operator A and re-train the DNN accordingly. In an attempt to remove artifacts generated by a GAN for an inverse imaging problem, one may want to experiment with improved cost functions that are regularly introduced in the literature, such as the popular WGANs [9], LSGANs [10], and cycle-consistent GANs [11].

While these approaches are sound course of actions, they possess the significant drawback of being excessively time-consuming and requiring large computational resources. Modifying the training procedures (such as gathering new training data or implementing new loss functions) of neural networks may take weeks, sometimes months, of research to converge to a satisfying product. In many settings, such as industry, this approach would not be an effective use of time. This also requires access to large computing power and training dataset, which a user may not necessarily have access to at test time. In addition, these approaches are not always guaranteed to succeed. Training with multiple degradation operators A does not include all possible operators encountered at test time. Similarly, even the most advanced types of GANs are far from being entirely immune to artifacts.

In this paper, we argue that in many cases, returning to time-consuming and heavy computing tasks such as pre-processing a dataset or re-training a DNN is unnecessary. If the trained DNN produces results of overall satisfying restoration quality despite the presence of mild artifacts, then these artifacts can be efficiently removed in a fully self-supervised and efficient fashion at test time.

More specifically, we propose to fine-tune the parameters $\tilde{\psi}$ of the DNN $f_{\tilde{\psi}}(\cdot)$ that produces sub-optimal results *without the use of a training dataset*. The supervision signal used for fine-tuning the parameters corresponds to the constraint that our observed test image y should be related to

the output of the DNN through the known image formation model: $Af_{\psi}(y) = y$. With this approach, noise patterns and artifacts that are not in agreement with the observed data will be penalized accordingly during fine-tuning. Thus as the parameters ψ of the DNN are updated to satisfy the data consistency constraint, they are displaced in parameter space in a direction that generates an improved solution $\hat{x} = f_{\hat{\psi}}(y)$. An illustration of our fine-tuning approach is shown in the blue box of Figure 1.

II. RELATED WORKS

Constraining the neural network solution to satisfy the data consistency term $Af_{\psi}(y) = y$ has become an increasingly popular trick in the literature of deep learning for inverse imaging problems. The constraint is in most cases implemented as non-trainable projection layers in the architecture of a neural network (see for example [12], [13], [14], [15]). These layers naturally map the output image of the DNNs onto the set of data consistent solutions and as a result, the network outputs solutions that are in agreement with the observed y .

To make image reconstruction networks robust to multiple image formation models, the literature typically designs new training datasets and strategies. For example, the authors of [16] found out that robustness to various degradation levels could be obtained by inserting a conditioning layer in their neural network architecture. At test time, the user selects a hyper-parameter that specifies the amount of degradation desired and adjusts the conditioning layer accordingly. In their work on video SR, the authors of [17] design a conditioning network that uses the pseudo-inverse image formation model to condition their super-resolving network and make it robust to multiple degradation models. While these strategies effectively produce networks that are robust to multiple types of forward models at test time, they still possess the drawback of requiring a significant amount of experimentation and training.

A recent approach in the image processing literature has been to fully depart from the definition of DNNs as learned mappings from degraded to restored images, and instead use un-trained DNNs as regularizers when inverting an observed image y using an analytical framework. A pioneer of this approach is the popular Deep Image Prior (DIP) [18] method, which defines the minimization problem $\hat{\theta} = \arg\min_{\theta} \|Ah_{\theta}(z) - y\|^2$ using a randomly initialized

neural network $h_\theta(\cdot)$, a fixed random input vector z , and the degradation operator A . Through the use of gradient descent, the algorithm eventually converges to a satisfactory restored image: $\hat{x} = h_{\hat{\theta}}(z)$. The supervision used during "training" is solely given by the data consistency constraint $Ah_{\hat{\theta}}(z) = y$. The authors of DIP claim that the architecture of $h_\theta(\cdot)$ is a strong enough regularizer to produce pleasing images without necessitating further regularization. Indeed, the obtained solutions in [18] look surprisingly similar to natural images.

Similarly, work in [19] on zero shot SR found out that one could successfully train a randomly initialized neural network using the internal data present in the low-resolution observation at test time. With a given low-resolution (LR) image, successive low and high resolution pairs are generated by successively downsampling the LR observation. The resulting pairs of higher and lower resolutions versions of that particular image are then used as sample pairs for training the neural network.

Our work differs from the previous literature [18], [19] in that our objective is not to train a randomly initialized DNN to super-resolve a given low-resolution observation. Instead, we consider the case in which we are provided with a deep neural network $f_{\tilde{\psi}}(\cdot)$ already trained for a specific image restoration task on a large dataset of input-output pairs. We focus on the case in which the network provides an overall suitable solution \tilde{x} , with the exception of generating mild artifacts in its output. Thus our method enhances the obtained solution by guiding the parameters of the trained neural network to agree with the data consistency term at test time.

In Section III, we describe in detail our approach for fine-tuning the parameters of the neural network by formulating an inversion problem at test time. We apply our method on the case in which the SR image formation model at test time does not match the one assumed for training in Section V. In Section VI, we show that our approach is effective at removing the artifacts produced by super-resolving GANs. We conclude this paper with a discussion in Section VII, which details the benefits and limitations of our proposed method. To the best of our knowledge, we are the first to establish a framework for image enhancement and artifact removal by fine-tuning the parameters of DNNs on the data consistency term.

III. PROPOSED METHOD

We first describe our justification (Section III-A) and framework (Section III-B) for fine-tuning a DNN at test time with the objective of enhancing the obtained solution $\tilde{x} = f_{\tilde{\psi}}(y)$.

A. Motivation

In the SR problem, the cost function \mathcal{C} used to train a DNN $f_{\tilde{\psi}}(\cdot)$ is often chosen to be the Mean-Squared-Error, with the optional inclusion of features and adversarial losses. This model embeds the estimation of the downsampling process in the function $f_{\tilde{\psi}}(y)$. A major disadvantage of

this approach is that the SR output does not satisfy the data consistency constraint, which may lead to subpar results such as SR images contaminated with undesirable artifacts. To resolve this, the authors of [12] train a network with the following SR solution:

$$g_\psi(y) = (I - A^+A)f_\psi(y) + A^+y, \quad (1)$$

where A^+ denotes the Moore-Penrose pseudoinverse of the degradation A . From this formulation it can be easily shown that the proposed SR solution $g_\psi(y)$ satisfies the data consistency problem, that is, $Ag_\psi(y) = y$. This new $g_\psi(y)$ solution may be seen as a mapping of the original $f_\psi(y)$ onto the set of plausible SR solutions given a fixed degradation operator A . The authors of [12] show that applying this constraint as a layer during training results in enhanced SR results and reduced artifacts. This approach was extended to VSR in [17].

However, as this approach requires the specification of a single degradation operator A , it is clear that it does not generalize to multiple image formation models or to the nature of the artifacts we would like to remove as a result of imperfect modeling during training. In fact, artifacts arising in the outputs of SR DNNs $f_\psi(\cdot)$ are rarely of the same kind, as they depend on the test image statistics, image formation model, or objective functions used during training. To illustrate this, we show in Figure 2 two examples of artifacts that were produced by VSR models later described in Section IV. The artifacts of Figure 2b corresponds to those obtained when using the wrong scale factor at test time (we discuss the removal of these distortions in Section V-A). The artifacts of Figure 2c arose as a result of complex GAN training dynamics, further described and corrected for in Section VI. It is clear from these two residual maps that these artifacts differ in type, scale, and location. Currently in the DNN literature and to the best of our knowledge, there exists no method that can successfully remove artifacts from a trained $f_\psi(\cdot)$ independently of the distortion type or image formation model without having to resort to a new training experiment or training dataset. However, our proposed method, detailed in the next section, is agnostic to the type, location, and nature of artifacts that may be produced by a trained $f_\psi(\cdot)$.

B. Fine-tuning on the data consistency term

Consider a super-resolving neural network $f_{\tilde{\psi}}(\cdot)$ trained on a large dataset (X, Y) with a cost function \mathcal{C} . This dataset is usually generated with the specification of one (or multiple) image formation models, $y = Ax$. Typically in super-resolution, the degradation operator A corresponds to a downsampling operator for a specific scale factor. As a result of training, we obtain the estimated parameters $\tilde{\psi}$ by solving $\tilde{\psi} = \underset{\psi}{\operatorname{argmin}} \mathbb{E}_{X, Y} \mathcal{C}(x, y, \psi)$ where the high and low-resolution pairs $x \sim X$ and $y \sim Y$ are sampled from the training dataset.

We propose a single, efficient framework for the case in which enhancing the artifacts-contaminated solution $\tilde{x} = f_{\tilde{\psi}}(y)$ is desirable, where y is the observed LR at test time. We

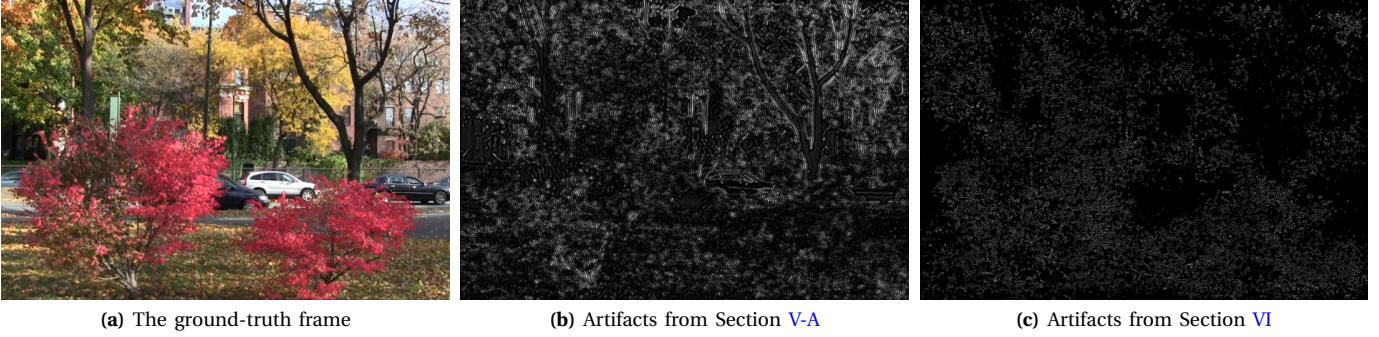


Figure 2: Examples of artifacts that may be produced by VSR models [5]. Figures (b) and (c) were obtained by computing the residual between the input $f_{\tilde{\psi}}(y)$ and output \hat{x} of our proposed fine-tuning algorithm $f_{\tilde{\psi}}$ for the experiments described in Sections V-A and VI .

argue that in such cases, one does not expect the ideal DNN parameters corresponding to an enhanced solution to lie far from the current parameters $\tilde{\psi}$ in parameter-space. With this in mind, we hypothesize that no extensive re-training is required in such cases. Instead, for a given LR observation, we need only to fine-tune the parameters in a direction for which the corresponding output image is enhanced. With an appropriately chosen supervision signal, the fine-tuned parameters converge to an enhanced solution in just a small number of iterations. Because artifacts are not consistent with the image formation model responsible for generating the LR observation, we argue that using our known formation model at test time to perform the fine-tuning of the DNN’s parameters naturally leads to an enhanced solution. Thus our cost function for fine-tuning becomes one that enforces consistency between the LR observation and the estimated $x = f_{\tilde{\psi}}(y)$ through the image formation model. To this end, we adapt the constraint originally formulated in Equation 1 as an optimization problem at test time:

$$\hat{\psi} = \arg \min_{\psi} \|A' f_{\psi}(y) - y\|_2^2, \quad (2)$$

where the starting vector ψ_0 for this optimization problem is set to $\tilde{\psi}$, and A' may differ from the A used to generate the training dataset (Section V). The pseudocode for solving Eq. 2 is shown in Algorithm 1.

We note here that our formulation in Equation 2 corresponds to the well established inversion problem posed by all image recovery tasks, which we apply here to the context of fine-tuning and output enhancement of an already trained network. While this supervision signal is very similar to the one used by the Deep Image Prior approach [18], our motivations for using it are distinct. We formulate the inversion problem as in Equation 2 not to restore an image from scratch as in DIP, but to enhance the solution supplied by a trained neural network. Our work thus combines the learning power of pre-trained DNNs with the dependability of analytical approaches for image restoration.

Computing the gradients of the terms in Equation 2 necessary to perform gradient descent is straightforward with the automatic differentiation functionalities offered by most Deep Learning libraries. As shown in Algorithm 1, we em-

ploy the Early Stopping [20] mechanism with the *patience* parameter set to 2 to interrupt the optimization process when the cost stops improving. We set the learning rate to $\alpha = 0.005$ and use the Stochastic Gradient Descent (SGD) optimizer in PyTorch [21]. No additional regularization is used. With the converged fine-tuned parameters $\hat{\psi}$, we then use $\hat{x} = f_{\hat{\psi}}(y)$ as the final enhanced, artifact-free solution.

Algorithm 1 Our proposed fine-tuning algorithm.

```

1: function FINETUNE( $\tilde{\psi}$ ,  $y$ ,  $A'$ )
2:    $\psi \leftarrow \tilde{\psi}$  ▷ Initialize parameters
3:    $earlyStop \leftarrow \text{False}$  ▷ Initialize stopping condition
4:   while  $earlyStop$  False do
5:      $x \leftarrow f_{\psi}(y)$  ▷ Forward pass
6:      $\mathcal{L} \leftarrow \|A'x - y\|_2^2$  ▷ Eq. 2
7:     Compute  $\nabla_{\psi} \mathcal{L}$  ▷ Backward pass
8:      $\psi \leftarrow \psi - \alpha \nabla_{\psi} \mathcal{L}$  ▷ Update weight
9:     update  $earlyStop$  ▷ True if  $\mathcal{L}$  increases
   return  $f_{\psi}(y)$ . ▷ Compute final SR

```

IV. ARCHITECTURES, EXPERIMENTAL DESIGN AND FIGURES OF MERIT

To demonstrate the effectiveness of our approach detailed in Section III, we perform a series of experiments on image and video SR models under various conditions. In Section IV-A, we introduce the SR neural networks used in our experiments. Section IV-B details the proposed experimental set-up and various use cases on which we apply our proposed algorithm. We conclude this section by defining the metrics used to quantitatively assess our results in Section IV-C.

A. Video and image SR architectures

To perform the video super-resolution (VSR) experiments presented in this paper, we obtain our pre-trained neural networks $f_{\tilde{\psi}}(\cdot)$ from [5] which introduces two models trained for the task of VSR for scale factor 4. In this paper, we refer to these two models as the VSRMSE model, trained with the Mean-Squared-Error loss $\mathcal{C} = \|f_{\tilde{\psi}}(y) - x\|_2^2$, and the VSRGAN model trained by introducing a discriminator

network g_ϕ with trainable parameters ϕ and using the cost function $\mathcal{C} = \log(1 - g_\phi(f_\psi(y)))$. Both the VSRMSE and VSRGAN architectures correspond to a Convolutional Neural Networks (CNNs) with 15 residual blocks (See Figure 1 in [5]). The input to both networks is a low-resolution video sequence $y = \{y_{t-2}, y_{t-1}, y_t, y_{t+1}, y_{t+2}\}$ and the output is the corresponding center high-resolution frame $x = x_t$.

While our proposed method is applied on models trained for *video* super-resolution, they are easily applicable to the problem of *image* super-resolution. Indeed, it is clear that our framework is agnostic to the input and output dimensionalities. This is further demonstrated in Section V-C, where we depart from our in-house VSR models and instead apply our fine-tuning method on the VDSR model [22], a state-of-the-art MSE-based still image SR neural network. The VDSR model is composed of 20 convolutional layers and a residual skip connection from input to output. We obtain the trained network by downloading the VDSR model weights and definitions at the *github* repository <https://github.com/twtygqyy/pytorch-vdsr>.

The VSRMSE, VSRGAN, and VDSR models require their low-resolution inputs to be brought to the same spatial extent as the high-resolution target image prior to being passed through the network. Thus our experiments apply MATLAB’s *imresize* function on the downsampled HR test image with the desired SR scale factor to obtain bicubically interpolated low-resolution image or frames prior to passing them through the networks.

B. Experiments

With these networks, we apply our fine-tuning algorithm described above on several case scenarios encountered when attempting to super-resolve LR data with SR DNNs. Section V tackles the scenario in which the image formation model at test time differs from the one assumed for training. More specifically in Section V-A, we show that our fine-tuning framework can successfully super-resolve LR images downsampled by a factor of 3 when the original network $f_\psi(\cdot)$ was originally super-resolving for scale factor 4. As SR models are seldomly trained for all scale factors (instead, a single network is re-trained for each scale factor), this scenario can be quite common. Section V-B handles the case in which Gaussian blur is part of the image formation model that generated the observed LR – an operation which was not accounted for during the training of the DNN. We will show that while the original output $\tilde{x} = f_\psi(y)$ is contaminated with a strong amount of smoothing, using the appropriate image formation model when fine-tuning with Equation 2 restores the inherent sharpness. This case scenario may also be quite frequent, as most of today’s Deep Neural Networks trained for super-resolution do not assume Gaussian blur in their formation model. Similarly in Section V-C, we consider the case when the user is provided with a test LR image that underwent an out-of-focus blur prior to being downsampled. We show that inputting this image to a neural network that was not trained with such blur results in slightly distorted textures. We show that

our proposed method can successfully restore the accurate structure in the output.

Unlike Section V, which addresses the case in which a different image formation model is used, the experiments in Section VI apply our fine-tuning approach with the purpose of removing artifacts that arise from a Generative Adversarial Network trained for super-resolution. Section VI-A provides insight into the cause of these artifacts by relating these to model uncertainty. Section VI-B introduces a *masked* variant of our fine-tuning algorithm, which was found to be a particularly effective approach for removing the artifacts generated by the GAN. The results of our fine-tuning procedure are detailed in Section VI-C.

C. Figures of merit

Below each of the figures presented in this paper, we display the corresponding quantitative metrics computed with respect to the known ground truth HR image. The first two metrics we report are the well-known objective image quality metrics, the PSNR and SSIM [23]. While these two metrics are the de facto standard metrics employed for assessing the performance of an image restoration model, they do not always provide an accurate assessment of the perceptual quality of images produced by deep neural networks. Therefore in addition to the PSNR and SSIM, we also provide the PercepDist metric proposed by [24]. This metric leverages the representations learned by CNNs to output a distance value between a reference and ground-truth image. The smaller the distance, the better the restoration quality. For more information regarding this metric, we refer the reader to [5], [25]. We remark here that while this metric’s popularity is increasing in the SR literature ([5], [26]), we did not find it to be *consistently* accurate in comparing the restoration quality of two images. Thus as any metric, the PercepDist is to be used in addition to a careful qualitative visual examination of the results.

V. FINE-TUNING FOR INCONSISTENT IMAGE FORMATION MODELS

We now consider the case in which the image formation model differs from the one assumed during training. In the next sections, we study the enhancement of sub-optimal images due to an unexpected change in scale factor (Section V-A), or due to the application of a Gaussian (Section V-B) and out-of-focus (Section V-C) blur operator.

A. Testing image with different downsampling factor

Our first experiment focuses on the case in which the downsampling operator at test time $y = D'x$ differs from the one assumed during training $y = Dx$. The D operator corresponds to bicubic downsampling for a specific scale factor. In this section, we employ the VSRMSE [5] trained to perform super-resolution for scale factor 4. It is reasonable to expect that at test time, inputting a LR video sequence that was downsampled by a factor other than 4 will result in the VSRMSE failing to produce clean super-resolved frames. In this section, we apply our method onto the

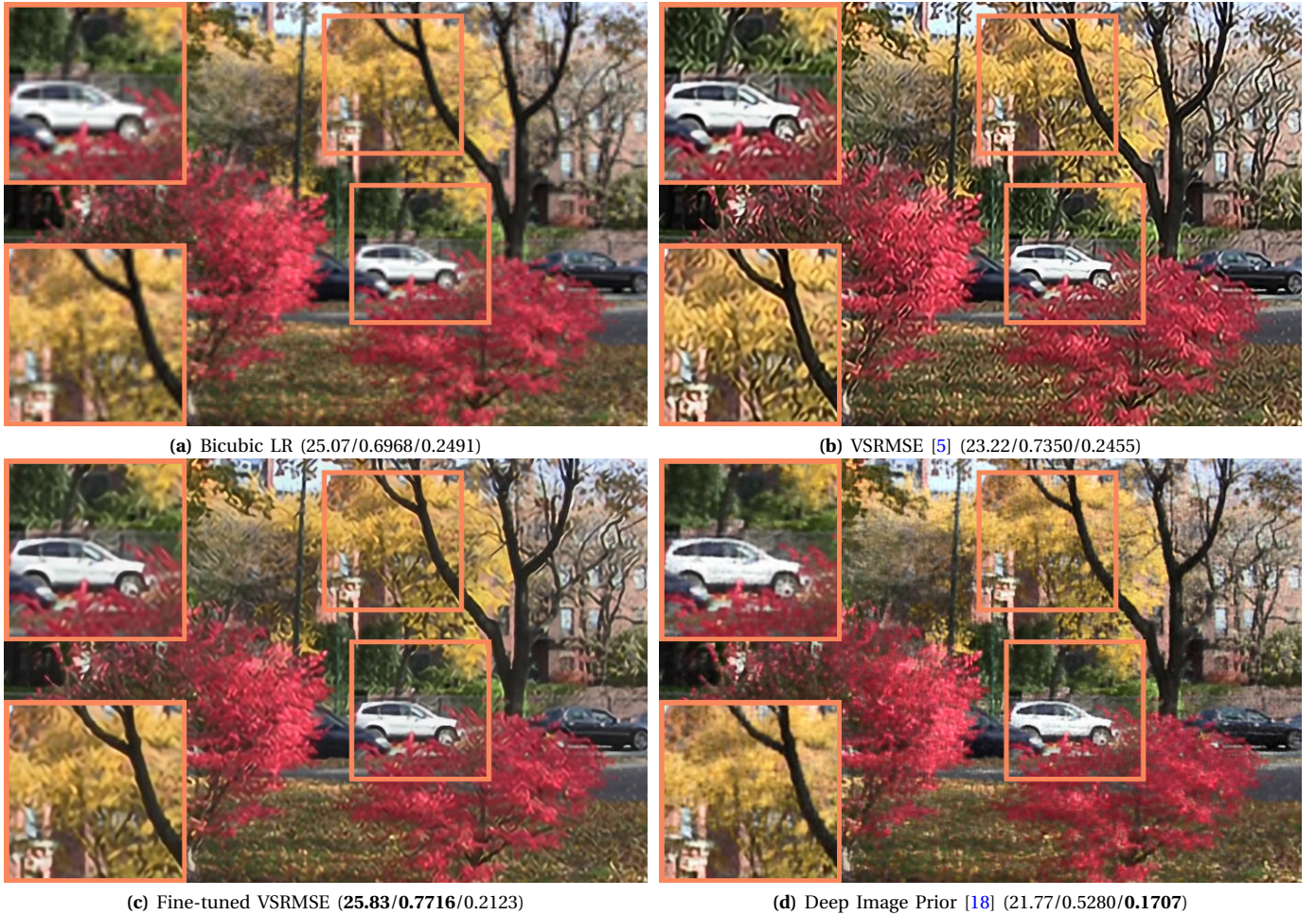


Figure 3: Fine-tuning the VSRMSE for testing on scale factor 3 SR when trained with scale factor 4. We show the result of DIP [18] for comparison. The frame corresponds to the "foliage" sequence of the Vidset4 test dataset.

"foliage" and "walk" sequences of the popular VidSet4 test dataset [27]. Figures 3b and 4b show the result of down-sampling the test video frames by 3 instead of 4 and super-resolving these with the trained VSRMSE. These figures show that while the VSRMSE was not trained for the VSR task of factor 3, it is remarkably successful at reducing the smoothness originally present in the bicubic low-resolution images shown in Figures 3a and 4a which were obtained by downsampling these by 3 and then upsampling them with *imresize*. Unfortunately, this increase in resolution is also accompanied with strong textural artifacts, particularly around the edges in Figures 3b and 4b. The resulting images overall look unrealistic and are thus unacceptable super-resolved solutions. Note that these observed distortions also result in a sharp decrease in PSNR values from Figures 3a and 4a to Figures 3b and 4b. Our main objective is to reduce the generated artifacts observed while keeping the increased resolution provided by VSRMSE. To this end, we apply the fine-tuning formulation introduced in Equation 2, where y is our video sequence downsampled by scale factor 3, $A' = D'$ is the bicubic downsampling operator for scale factor 3 and the $f_{\hat{\psi}}(\cdot)$ network is the trained VSRMSE network for scale factor 4. We set the parameters ψ_0 at

the first iteration to correspond to the pre-trained VSRMSE $\tilde{\psi}$ parameters. As a result of fine-tuning, we are provided with our new parameters $\hat{\psi}$ and thus generate a new solution $\hat{x} = f_{\hat{\psi}}(y)$, displayed in Figure 3c and 4c. From these figures we observe that our fine-tuning method successfully removes the ringing artifacts while maintaining the initially acquired high resolution of Figures 3b and 4b. In addition to this qualitative improvement, applying our algorithm resulted in an important PSNR increase of 2.61 dB for the "foliage" frame in Figure 3 and of 2.38 dB for the "walk" frame in Figure 4. Similarly, the PercepDist value underwent a significant decrease for both frames, an improvement that is consistent with our qualitative observations.

Furthermore, to demonstrate the effectiveness of fine-tuning as opposed to starting from scratch, we compare our results with those obtained from running the DIP [18] code provided by the authors at <https://github.com/DmitryUlyanov/deep-image-prior>, modified for performing super-resolution for scale factor 3. Because the DIP network requires a single image input as opposed to a video sequence as required by VSRMSE, we modify the code as to super-resolve the center frame of our video sequence. Figures 3d and 4d reveal that the resulting



Figure 4: Fine-tuning the VSRMSE network for testing on scale factor 3 SR when trained with scale factor 4. We show the result of DIP [18] for comparison. The frame corresponds to the "walk" sequence of the Vidset4 test dataset.

image has a grainy/noisy texture and an overall blurrier nature that is not present in our fine-tuned solution.

We conclude this section by noting that our method is also successful at removing strong artifacts resulting from images that have been downsampled by a factor of 2 as opposed to 3; however, we are not including the resulting figures in this paper due to space limitations. For these set of experiments, the PSNR improved by 7.32 dB for the "foliage" sequence and 5.30 dB for the "walk" sequence. Large improvements in the PercepDist and SSIM metrics were observed as well.

B. Testing image with Gaussian smoothing

The previous section assumed a forward process in which the high-resolution image is downsampled with bicubic downsampling, i.e., $y = Dx$. This coincides with today's prevailing approach in DL to generating pairs of high and low-resolution images with such a formation model. However, a more general and accurate model for SR is one in which blur is applied prior to downsampling, i.e. $y = DBx$. Indeed low-resolution images may also suffer from blur for example due to motion, optics, sensor, or atmospheric turbulence [28]. In these cases, super-resolving such images with a

Deep Neural Network trained without taking such possible blur deformations into account will result in various types of artifacts at the output.

In this section, we apply a 2-D Gaussian smoothing kernel with standard deviation of 2.0 prior to the bicubic downsampling operator to obtain our low-resolution test sequences y . We show the resulting bicubically interpolated low-resolution frame in Figure 5a. We provide this input to VSRMSE and obtain the solution shown in Figure 5b. While we notice a sharp improvement in PSNR and PercepDist, the resulting output \hat{x} still suffers from excessive smoothing. We show as a means of comparison the result of super-resolving an LR frame for which Gaussian blur was not part of its image formation model, shown in Figure 5d. Comparing this with Figure 5b reveals that the VSRMSE model was not effective at super-resolving the blurred low-resolution image. This is of course not unexpected, as the training dataset used to train the VSRMSE did not contain LR images contaminated with blurring in addition to downsampling, thus the model did not learn the appropriate mapping from low to high-resolution.

Our objective is to obtain results that are quantitatively and qualitatively closer to those of Figure 5d, results ob-

tained when no blurring is applied to the inherent high-resolution x . The traditional approach is to return to the pre-processing stage, define a new image formation model which this time includes Gaussian blur, and re-train the model on the new dataset. Instead, we show that we can bypass this lengthy process and almost effortlessly improve our results with our fine-tuning algorithm. We define $A' = \text{DB}$ in Equation 2 and fine-tune the parameters of the neural network accordingly. The result of our algorithm \hat{x} displayed in Figure 5c demonstrates a significant increase in resolution compared with the obtained initial prediction in Figure 5b. These observations are consistent with the improved quantitative metrics shown below each figure, demonstrating an increase of 1.42 dB in PSNR and a sharp decrease of 0.0687 in terms of the PercepDist metric.

C. Testing image with out-of-focus blur

The previous section focused on enhancing SR results for inputs that had undergone Gaussian smoothing at test time. In this section, we still consider the case in which the test image formation model is $y = \text{DB}x$ instead of $y = \text{D}x$. However, the blur operator B now corresponds to an out-of-focus blur as opposed to the previously assumed Gaussian blur. In the subsequent experiment, we model out-of-focus blur with the use of a circular point spread function (PSF) of radius $r = 2$.

To show that our algorithm is not specific to our VSRMSE model or the video SR task, we temporarily depart from the VSRMSE model and instead borrow the VDSR [22] model trained for single image SR for scale factor 2. Because the VDSR model is trained for image super-resolution, testing on the VidSet4 sequences is no longer applicable. Instead, we obtain two test images from the *Set5* and *Urban100* image databases, commonly used to test single image SR models [29]. We obtain our LR images by convolving our circular PSF with the original HR image and downsampling them by a factor of 2.

Equipped with the VDSR model, we super-resolve our blurry LR images and show the results in Figures 6b and 6e. We contrast these results with the corresponding ground-truth images shown in Figures 6a and 6d. Comparing these reveal that super-resolving out-of-focus LR images with a network that did not expect such blur results in a loss of fidelity to the ground-truth texture. This is particularly noticeable in the highlighted regions of Figures 6b and 6e. It is clear that the fine-grained textures are not accurately super-resolved and instead seem distorted when compared with their ground-truth counterparts.

We thus apply our fine-tuning framework to enhance the resulting images and remove the displeasing effect of applying the out-of-focus blur at test time. We show the results of our algorithm in Figures 6c and 6f. A qualitative assessment of these figures reveals that the inherent ground-truth texture is accurately recovered as a result of applying our fine-tuning algorithm. Our quantitative measurements agree with these qualitative observations, demonstrating an increase of over 1.0 dB in the PSNR metric.

In this section we have shown how to handle mismatches between image formation models at training and test time. In the next section, we apply our fine-tuning algorithm introduced in III to reduce artifacts that arise from the training dynamics specific to Generative Adversarial Networks.

VI. FINE-TUNING FOR THE REMOVAL OF GAN ARTIFACTS

Generative Adversarial Networks (GANs) have become an increasingly popular tool for super-resolving images and videos. Often combined with perceptual losses [30], these adversarially trained networks are trained to accept a LR image as their input and make the SR output appear *as if* it was sampled from the high-resolution data [4], [31]. Despite their success in generating highly realistic images, Generative Adversarial Networks trained for super-resolution applications often suffer from introduced undesirable artifacts [5], [31].

The experiment described in this section exploits the VSRGAN model introduced in Section IV. This GAN-based model demonstrates strong restoration capabilities with the exception of introducing minor artifacts in the SR solution [5]. For a given test LR, we apply our proposed algorithm on VSRGAN parameters and show that the fine-tuned parameters produce an artifact-free super-resolved image of high photo-realistic quality. In Section VI-A, we build on recent research on model uncertainty and introduce a novel approach to automatically locate the undesirable artifacts in a SR image generated by VSRGAN. Using these results, Section VI-B presents a masked variant of our fine-tuning algorithm that makes use of the known artifact location to improve results. Finally, our results are detailed in Section VI-C. We remark here that while our experiments focus on the VSRGAN model, our method is model agnostic and thus can be generalized to any GAN-based model which produces mild artifacts in the SR solution.

A. Location of the artifacts with model uncertainty

Discriminative Deep Neural Networks trained for image classification tasks have recently received a lot of attention, particularly since they were found to be prone to adversarial attacks, attacks that tailor small changes in the input image with the objective to fool the DNN classifier [32], [33]. These attacks are created by adding a small perturbation to a normal image which causes the classifier to misclassify the sample, but does not look different to the human eye. These harmful input images are often referred to as adversarial inputs, or adversarial samples, in the literature. To prevent such deceitful classifications, numerous works in the current literature are now focusing on the development of methods that automatically detect adversarial inputs [34], [35]. The authors of [35] found that higher levels of uncertainty in the DNN's output were correlated with the presence of an adversarial sample at its input. Thus the authors propose to use dropout [36], a regularization layer that has been linked with Bayesian uncertainty estimation [37], to quantify the uncertainty of a DNN's prediction for a given input and use the results as a means to detect



Figure 5: Testing the VSRMSE network on a LR input which was blurred with a Gaussian blur before being downsampled. We show the result of super-resolving a non-blurred LR with VSRMSE for comparison.

adversarial attacks. Below, we propose to take a similar approach to assess VSRGAN’s uncertainty in its prediction and locate its generated artifacts

Examples of artifacts generated by GANs for VSR are shown in Figures 7b, 7e and 8b. While these frames appear to be of strong super-resolved quality, a closer look at these figures reveals the presence of a "dot-like" noise pattern, made evident in the zoomed-in regions. In [5] we hypothesized that during training, the VSRGAN (erroneously) learns that these artifacts are suitable high-frequency signals to generate in a SR frame. Viewing the videos super-resolved by VSRGAN revealed a significant amount of flickering of these artifacts across consecutive frames. This severe lack of motion consistency of the generated noise suggests a possible relationship between model uncertainty and the produced artifacts. We thus hypothesize that our trained VSRGAN model and possibly other GAN-based models, suffer, too, from model uncertainty when producing the dot-pattern noise in the super-resolved pixels.

To visualize VSRGAN’s uncertainty, we build on the work in [35] and insert dropout layers in VSRGAN at test time to insert randomness into our model and study the consistency of its prediction across multiple forward passes.

We add dropout layers in between each of the residual blocks and set the probability of dropping out corresponding neurons at $p = 0.0005$. We note here that while the VSRGAN architecture does not originally contain dropout layers, no re-training stage is required here. At test time, given an LR input, we perform 50 forward passes with our VSRGAN-dropout model and compute the pixel-wise variance across the 50 predicted frames. According to [35], higher levels of variance in a region of the super-resolved frame suggests lower confidence in the model’s prediction. We show such a computed variance map for two different LR inputs in Figures 7a and 7d (for visualization purposes, we show high variance points in black pixels, whereas low variance points are encoded in white). Viewing this variance map reveals that model uncertainty is far from being uniform across the predicted pixels. More particularly, high variance regions seem to correspond to the location of the produced artifacts. This observation reinforces our earlier hypothesis that generated artifacts are associated with lower confidence levels of VSRGAN. In the next section, we exploit this finding to develop a masked formulation of our fine-tuning algorithm.

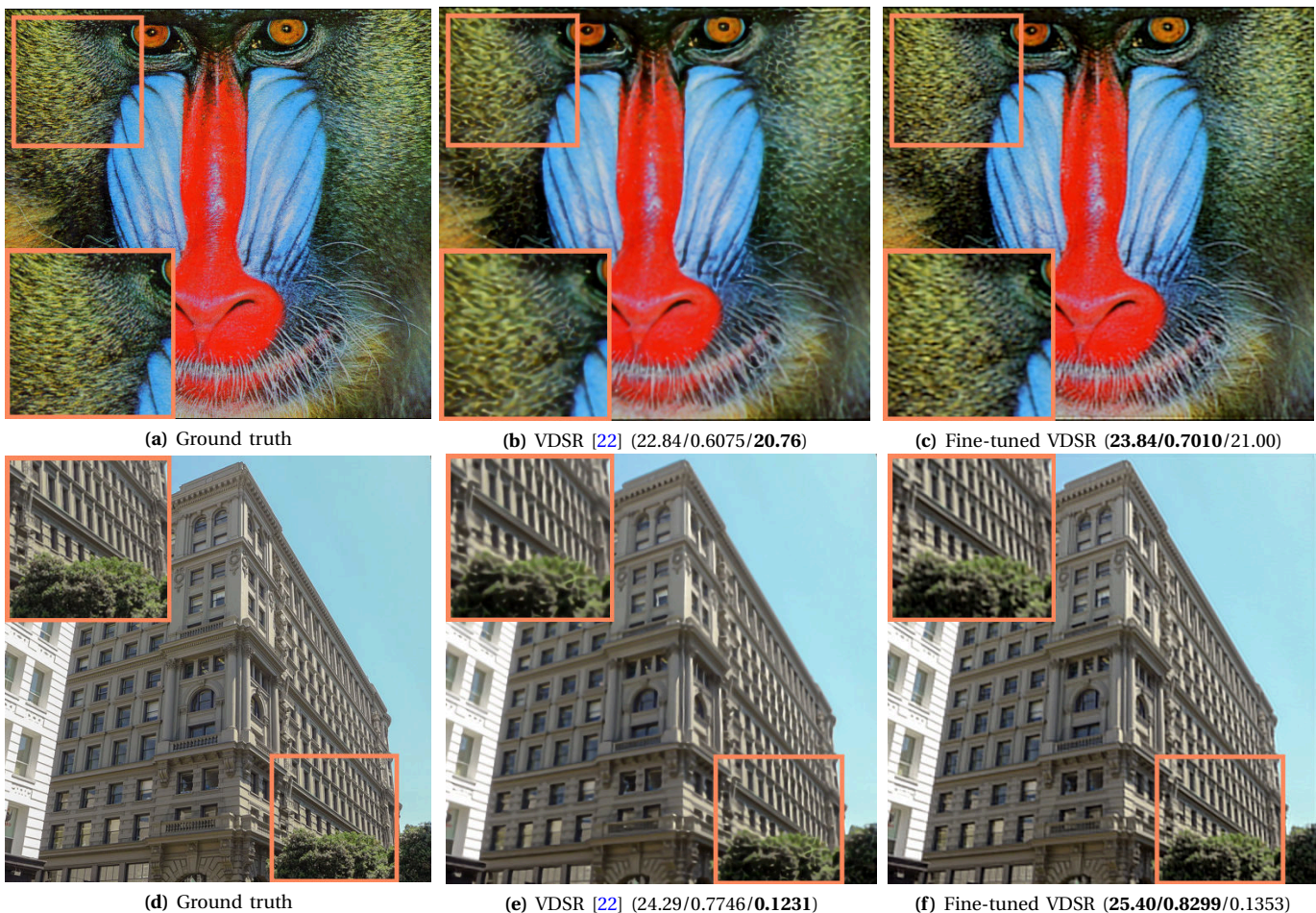


Figure 6: Testing the VDSR network on a LR input which was blurred with an out-of-focus blur before being downsampled.

B. A masked formulation of our fine-tuning method

The VSRGAN super-resolved frames in Figures 7b, 7e and 8b reveal that the pixels contaminated with artifacts are located in regions of complex textures, which also correspond to regions of high uncertainty as explained in the previous section. Other areas of the SR frames are clean and free from generated noise. To obtain an optimal fine-tuned solution, we argue that our optimization problem should fully exploit the information present in the problematic regions when computing gradient updates and to some extent ignore the clean regions in the SR frame. To this end, we assume access to a binary mask M that encodes the pixel-wise location of the artifacts and re-formulate our optimization problem for GAN artifact removal as:

$$\hat{\psi} = \arg \min_{\psi} \|A'(f_{\psi}(y) \odot M) - y \odot M_d\|_2^2 \quad (3)$$

Here \odot denotes the element-wise multiplication operation and M_d is the downsampled version of M . The next section details how to estimate M from the dropout variance map described in Section VI-A. The new optimization problem in Eq. 3 mainly differs from the original formulation in Eq. 2 in that the mask M effectively places a higher penalty on the parameters that are responsible for producing the

artifacts in the SR frame. Thus our optimization focuses on enhancing the problematic regions identified by $f_{\psi}(y) \odot M$ and comparing them with the corresponding ground-truth LR pixels $y \odot M$. Obtaining the new computed $\hat{\psi}$ parameters from Eq. 3, we then define our final fine-tuned solution as:

$$\hat{x} = f_{\hat{\psi}}(y) \odot M + f_{\hat{\psi}}(y) \odot (1 - M) \quad (4)$$

This residual formulation essentially corrects for the pixels that had been identified as corrupted by replacing them with the new $f_{\hat{\psi}}(y) \odot M$ while preserving the clean pixels $f_{\hat{\psi}}(y) \odot (1 - M)$ in the rest of the original image. As a result, our fine-tuned SR frame successfully maintains its original super-resolved quality with the absence of the dot-pattern noise. In the next section, we apply Eq. 3 on our VSRGAN frames and detail our results.

C. Experimental Results

Let us first describe how to derive the binary mask M in Equations 3 and 4 from the dropout variance maps described in Section VI-A, which we denote in this section as V . To binarize our variance map V , we first compute the mean pixel-value m of V and set all pixels in M that have a value above m to 1, and all others to 0, i.e., $M(V \geq m) = 1$ and $M(V < m) = 0$. To obtain a clean binary mask, we then

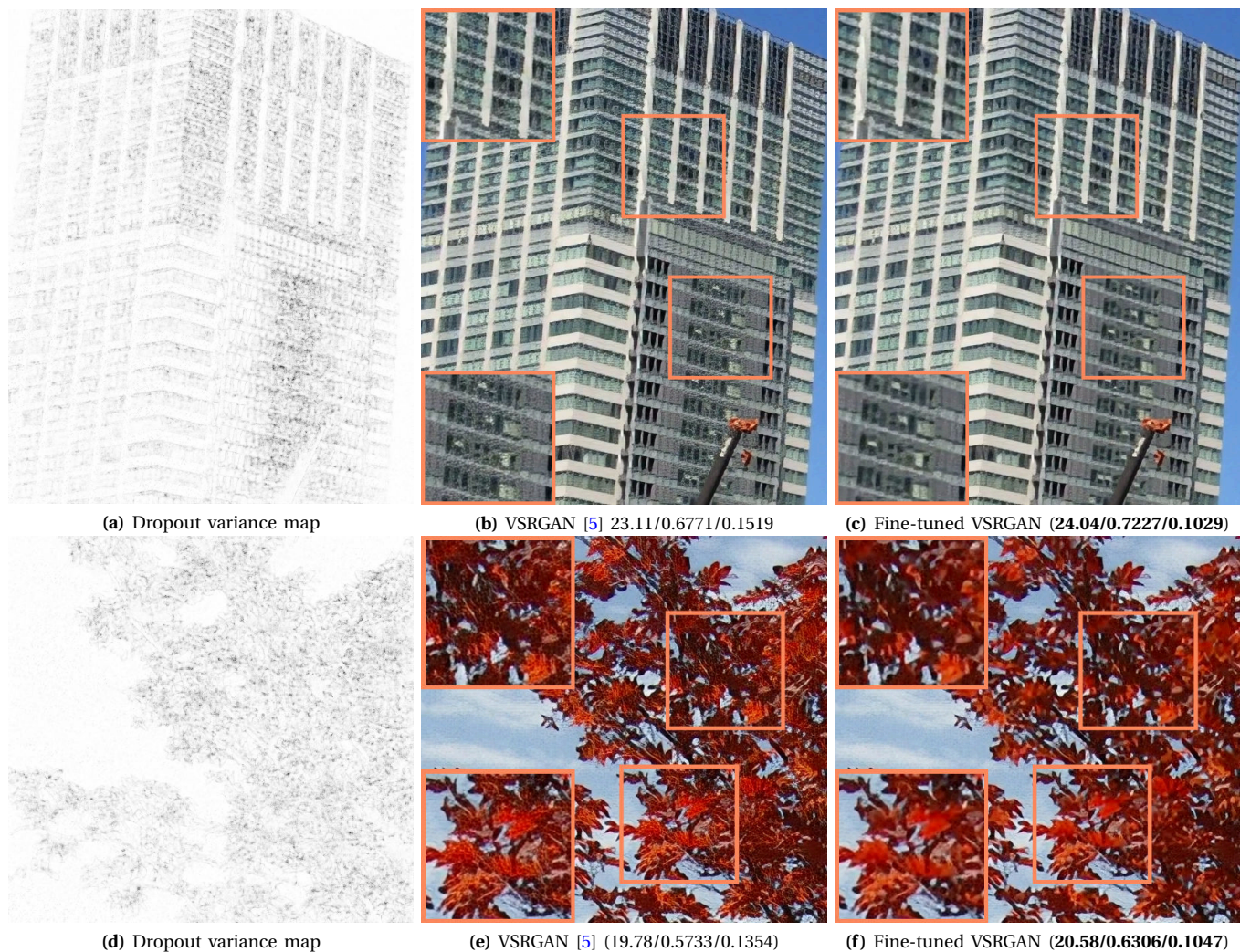


Figure 7: Fine-tuning VSRGAN.



Figure 8: Fine-tuning VSRGAN. The fine-tuned result accurately recovers the structure in (a).

filter out isolated 1's in the computed mask M by applying a median filter with kernel size 3.

Equipped with a binary mask M for each of our test frames, we apply Equation 3 to the images produced by our VSRGAN model, trained for the SR problem of scale factor 4. Our final fine-tuned results are computed by applying the residual formulation of Equation 4 and shown in Figures 7c, 7f, and 8c. Comparing these with Figures 7b, 7e and 8b demonstrates the successful removal of the strong dot-pattern artifacts originally observed. In addition to providing a cleaner look to the SR frames, our fine-tuning approach presents the additional benefit of restoring the inherent ground-truth pattern in the SR prediction. This is made particularly evident in Figure 8. Indeed, a comparison

of Figure 8b with the ground-truth frame shown in Figure 8a reveals that the VSRGAN $f_{\psi}(\cdot)$ wrongly opted to generate a heavy squared-like texture on the roof of the building. While the super-resolved frame appears at first to be of high super-resolved quality, it fails to preserve the authentic pattern present in the ground-truth frame. As a result of applying our fine-tuning algorithm, shown in Figure 8c, the inherent ground-truth structure is recovered from the low-resolution observation.

The quantitative measurements shown below each example are consistent with our qualitative observations. Both test frames shown in Figures 7c and 7f experienced an increase in PSNR of 0.93 dB and 0.80 dB, respectively, while Figure 8c underwent an important increase of 1.53 dB. Significant

improvements in the PercepDist metric are also observed for all three frames as well.

VII. DISCUSSION

The experimental results presented in Sections V and VI demonstrated that our proposed fine-tuning algorithm successfully suppresses artifacts (Sections V-A, V-C, VI-C) and/or sharpens images (Section V-B) under various conditions. In addition to the clear qualitative improvements, quantitative gains in PSNR, SSIM and PercepDist were consistently observed for each of the detailed experiments. The fact that the PSNR and PercepDist metrics simultaneously increased confirms our algorithm’s two-folds ability in increasing (1) the result’s fidelity to the ground truth observation and (2) the photorealistic quality of the test image.

We must emphasize here that the applicability of our proposed method is not limited to the experiments described in this paper. Indeed, our fine-tuning algorithm for image enhancement is agnostic to the inverse imaging problem at hand, the artifacts encountered or their origin. An observed test image, a known image formation model and a pre-trained neural network $f_{\tilde{y}}(\cdot)$ are the only components required for applying Algorithm 1. Furthermore, while we presented our fine-tuning approach in its most elementary form, more evolved variants of our proposed method may be easily derived to better suit other imaging problems. The medical imaging community, for example, may want to incorporate additional regularizers in Equation 2 to enforce prior knowledge of the image’s expected characteristics, for example enforcing a sparse representation in a given domain. Similarly, a variant of our algorithm was introduced in (Section VI-B) of our paper, where we presented a masked formulation of our method with the use of dropout variance masks to address the case in which artifacts arise from lack of model confidence.

Perhaps the strongest feature of our proposed framework is its exceptional time and storage efficiency, removing the need to synthesize new training data or perform lengthy training experiments, both of these stages being tedious and not guaranteed to succeed. The average user may also not have access to such computational resources to perform such tasks. Our algorithm, however, fully and efficiently operates at test time. In the experiments described in Section V-A, for example, fine-tuning our network with the Early Stopping criterion is completed in less than 4 seconds when implemented on a GTX 1080 GPU. On the other hand, the image restored by the DIP [18] method shown in Figure 3d requires a total of 25 minutes of computation on the same GPU card. This latter observation is not unexpected, as the DIP approach trains a network from scratch given the low-resolution observation, while we perform a few gradient updates on an already trained network.

As any new proposed framework, our method has its limitations and thus could benefit from further improvement. For example, our method is currently restricted to non-blind problems, in which the forward model is known. An existing workaround solution is to combine our approach

with an off-the-shelf algorithm that identifies the unknown A and then use this estimation in Equation 2. For example, the knowledge of the blur matrix B in SR is not always guaranteed in most situations. In such cases, B can be reasonably approximated using any of the techniques proposed in [28], [38], [39], [40] and then used by our proposed framework. Similarly, another limitation of our algorithm is its requirement that the degradation operator A' in Eq. 2 is to be written in matrix form, which certainly is not achievable for all imaging problems.

Finally our proposed framework still presents room for improvement in that it is not fully automated and still requires some amount of hyper-tuning, e.g., to select the ideal learning rate and/or gradient descent algorithm, or the threshold condition for producing the mask M in Section VI-B. However, it is clear that the amount of work associated with these hyper-parameter decisions is minuscule compared to those required for re-training a neural network to obtain the appropriate solution.

VIII. CONCLUSION

In this work, we proposed a fine-tuning algorithm to post-process sub-optimal images generated by DNNs for the SR problem. We achieve this by fine-tuning the parameters of our neural networks to satisfy a data consistency term given a new test data point. Our method is fully self-supervised and distinguishes itself in that it does not necessitate large training datasets or evolved training experiments to be effective. We applied our algorithm to various models and case scenarios. In each of our experiments, our approach consistently resulted in images of higher qualitative and quantitative quality.

Post-processing the solutions of DNNs using fine-tuning on a test input image is a topic that has so far not been explored in the literature, other than in our initial work presented in [1]. The novelty of our approach naturally provides room for further research and improvement on our proposed framework. An example of such improvements may be obtained by combining the abundant research in analytical methods for inverse imaging problems with efficient fine-tuning in pre-trained parameter space. One could also easily introduce additional regularizers to the proposed framework, which may be particularly beneficial to communities such as the medical imaging community. Investigating further in such directions will provide deep learning scientists with more leeway to address some of the shortcomings of deep learning. Indeed, through the application of reliable, well-established analytical approaches offered by the image processing community to this framework, one may be one step closer to achieving restorations of previously unseen quality produced by DNNs for inverse imaging problems.

REFERENCES

- [1] A. Lucas, S. Lopez-Tapia, R. Molina, and A. K. Katsaggelos, "Efficient fine-tuning of neural networks for artifact removal in deep learning for inverse imaging problems," in *IEEE International Conference on Image Processing*, 2019.
- [2] A. Lucas, M. Iliadis, R. Molina, and A. K. Katsaggelos, "Using deep neural networks for inverse problems in imaging: beyond analytical methods," *IEEE Signal Processing Magazine*, vol. 35, no. 1, pp. 20–36, 2018.
- [3] G. Riegler, S. Schuler, M. R  ther, and H. Bischof, "Conditioned regression models for non-blind single image super-resolution," in *2015 IEEE International Conference on Computer Vision (ICCV)*, pp. 522–530, Dec 2015.
- [4] I. Goodfellow, J. Pouget-Abadie, M. Mirza, B. Xu, D. Warde-Farley, S. Ozair, A. Courville, and Y. Bengio, "Generative adversarial nets," in *Advances in neural information processing systems*, pp. 2672–2680, 2014.
- [5] A. Lucas, S. Lopez-Tapia, R. Molina, and A. K. Katsaggelos, "Generative adversarial networks and perceptual losses for video super-resolution," *IEEE Transactions on Image Processing*, vol. 28, no. 7, pp. 3312–3327, 2019.
- [6] A. Lucas, A. K. Katsaggelos, S. Lopez-Tapia, and R. Molina, "Generative adversarial networks and perceptual losses for video super-resolution," in *IEEE International Conference on Image Processing*, 2018.
- [7] C. Ledig, L. Theis, F. Husz  r, J. Caballero, A. Cunningham, A. Acosta, A. Aitken, A. Tejani, J. Totz, Z. Wang, *et al.*, "Photo-realistic single image super-resolution using a generative adversarial network," *arXiv preprint*, 2017.
- [8] X. Wang, K. Yu, S. Wu, J. Gu, Y. Liu, C. Dong, Y. Qiao, and C. Loy, "Esrgan: Enhanced super-resolution generative adversarial networks," in *European Conference on Computer Vision*, pp. 63–79, Springer, 2018.
- [9] M. Arjovsky, S. Chintala, and L. Bottou, "Wasserstein gan," *arXiv preprint arXiv:1701.07875*, 2017.
- [10] X. Mao, Q. Li, H. Xie, R. Lau, Z. Wang, and S. Smolley, "Least squares generative adversarial networks," in *Proceedings of the IEEE International Conference on Computer Vision*, pp. 2794–2802, 2017.
- [11] J.-Y. Zhu, T. Park, P. Isola, and A. Efros, "Unpaired image-to-image translation using cycle-consistent adversarial networks," *arXiv preprint*, 2017.
- [12] C. K. S  nderby, J. Caballero, L. Theis, W. Shi, and F. Husz  r, "Amortised map inference for image super-resolution," *arXiv preprint arXiv:1610.04490*, 2016.
- [13] S. Lopez-Tapia, A. Lucas, R. Molina, and A. K. Katsaggelos, "Gan-based video super-resolution with direct regularized inversion of the low-resolution formation model," in *IEEE International Conference on Image Processing*, 2019.
- [14] J. Schlemper, J. Caballero, J. Hajnal, A. Price, and D. Rueckert, "A deep cascade of convolutional neural networks for dynamic mr image reconstruction," *IEEE transactions on Medical Imaging*, vol. 37, no. 2, pp. 491–503, 2018.
- [15] K. Hammernik, T. Klatzer, E. Kobler, M. Recht, D. Sodickson, T. Pock, and F. Knoll, "Learning a variational network for reconstruction of accelerated mri data," *Magnetic resonance in medicine*, vol. 79, no. 6, pp. 3055–3071, 2018.
- [16] J. He, C. Dong, and Y. Qiao, "Modulating image restoration with continual levels via adaptive feature modification layers," in *Proceedings of the IEEE Conference on Computer Vision and Pattern Recognition*, pp. 11056–11064, 2019.
- [17] S. Lopez-Tapia, A. Lucas, R. Molina, and A. K. Katsaggelos, "Multiple-degradation video super-resolution with direct inversion of the low-resolution formation model," in *European Signal Processing Conference*, 2019.
- [18] D. Ulyanov, A. Vedaldi, and V. Lempitsky, "Deep image prior," in *Proceedings of the IEEE Conference on Computer Vision and Pattern Recognition*, pp. 9446–9454, 2018.
- [19] A. Shocher, N. Cohen, and M. Irani, "'zero-shot' super-resolution using deep internal learning," in *Proceedings of the IEEE Conference on Computer Vision and Pattern Recognition*, pp. 3118–3126, 2018.
- [20] F. Girosi, M. Jones, and T. Poggio, "Regularization theory and neural networks architectures," *Neural computation*, vol. 7, no. 2, pp. 219–269, 1995.
- [21] A. Paszke, S. Gross, S. Chintala, G. Chanan, E. Yang, Z. DeVito, Z. Lin, A. Desmaison, L. Antiga, and A. Lerer, "Automatic differentiation in pytorch," *31st Conference on Neural Information Processing Systems (NIPS 2017)*, 2017.
- [22] J. Kim, J. Kwon Lee, and K. Mu Lee, "Accurate image super-resolution using very deep convolutional networks," in *Proceedings of the IEEE Conference on Computer Vision and Pattern Recognition*, pp. 1646–1654, 2016.
- [23] A. Hore and D. Ziou, "Image quality metrics: Psnr vs. ssim," in *2010 20th International Conference on Pattern Recognition*, pp. 2366–2369, IEEE, 2010.
- [24] R. Zhang, P. Isola, A. A. Efros, E. Shechtman, and O. Wang, "The unreasonable effectiveness of deep networks as a perceptual metric," in *Proceedings of the IEEE Conference on Computer Vision and Pattern Recognition*, 2018.
- [25] K. Zhang, W. Zuo, and L. Zhang, "Learning a single convolutional super-resolution network for multiple degradations," in *Proceedings of the IEEE Conference on Computer Vision and Pattern Recognition*, pp. 3262–3271, 2018.
- [26] E. P  rez-Pellitero, M. S. Sajjadi, M. Hirsch, and B. Sch  lkopf, "Photorealistic video super resolution," *arXiv preprint arXiv:1807.07930*, 2018.
- [27] C. Liu and D. Sun, "A bayesian approach to adaptive video super resolution," in *Proceedings of the IEEE Conference on Computer Vision and Pattern Recognition*, pp. 209–216, IEEE, 2011.
- [28] M. Elad and A. Feuer, "Restoration of a single superresolution image from several blurred, noisy, and undersampled measured images," *IEEE transactions on image processing*, vol. 6, no. 12, pp. 1646–1658, 1997.
- [29] C. Dong, C. C. Loy, K. He, and X. Tang, "Learning a deep convolutional network for image super-resolution," in *European Conference on Computer Vision*, pp. 184–199, Springer, 2014.
- [30] J. Johnson, A. Alahi, and L. Fei-Fei, "Perceptual losses for real-time style transfer and super-resolution," in *European Conference on Computer Vision*, pp. 694–711, Springer, 2016.
- [31] C. Ledig, L. Theis, F. Husz  r, J. Caballero, A. Cunningham, A. Acosta, A. Aitken, A. Tejani, J. Totz, Z. Wang, *et al.*, "Photo-realistic single image super-resolution using a generative adversarial network," *arXiv preprint arXiv:1609.04802*, 2016.
- [32] N. Papernot, P. McDaniel, X. Wu, S. Jha, and A. Swami, "Distillation as a defense to adversarial perturbations against deep neural networks," in *2016 IEEE Symposium on Security and Privacy (SP)*, pp. 582–597, IEEE, 2016.
- [33] A. Madry, A. Makelov, L. Schmidt, D. Tsipras, and A. Vladu, "Towards deep learning models resistant to adversarial attacks," *arXiv preprint arXiv:1706.06083*, 2017.
- [34] W. Xu, D. Evans, and Y. Qi, "Feature squeezing: Detecting adversarial examples in deep neural networks," *arXiv preprint arXiv:1704.01155*, 2017.
- [35] R. Feinman, R. R. Curtin, S. Shintre, and A. B. Gardner, "Detecting adversarial samples from artifacts," *arXiv preprint arXiv:1703.00410*, 2017.
- [36] N. Srivastava, G. Hinton, A. Krizhevsky, I. Sutskever, and R. Salakhutdinov, "Dropout: a simple way to prevent neural networks from overfitting," *The Journal of Machine Learning Research*, vol. 15, no. 1, pp. 1929–1958, 2014.
- [37] Y. Gal and Z. Ghahramani, "Dropout as a bayesian approximation: Representing model uncertainty in deep learning," in *international conference on machine learning*, pp. 1050–1059, 2016.
- [38] S. Harmeling, S. Sra, M. Hirsch, and B. Sch  lkopf, "Multiframe blind deconvolution, super-resolution, and saturation correction via incremental em," in *IEEE International Conference on Image Processing*, pp. 3313–3316, Sep. 2010.
- [39] T. Michaeli and M. Irani, "Nonparametric blind super-resolution," in *IEEE International Conference on Computer Vision*, pp. 945–952, Dec 2013.
- [40] Q. Wang, X. Tang, and H. Shum, "Patch based blind image super resolution," in *IEEE International Conference on Computer Vision*, vol. 1, pp. 709–716 Vol. 1, Oct 2005.